2022 IEEE International Conference on Robotics and Automation (ICRA)
May 23-27, 2022. Philadelphia, PA, USA

# Design and Modeling of a Compact Advancement Mechanism for a Modified COAST Guidewire Robot

Patrick Lis*, Achraj Sarma, Grace Trimpe†, Timothy A. Brumfiel,
Ronghuai Qi, and Jaydev P. Desai, *Fellow IEEE*

***Abstract*— Peripheral vascular intervention remains a challenging procedure mainly due to the tortuosity of the vessels needing to be traversed by guidewires and catheters. In addition, handling long guidewires while navigating tortuous vasculature requires extensive time and skill from the surgeon. In this work, a compact guidewire advancement mechanism is proposed that is able to dispense guidewires up to 150 cm in length. The mechanism is adapted to actuate a prototype of the modified COaxially Aligned STeerable (COAST) guidewire robot to perform follow-the-leader (FTL) motion. The design of this mechanism consists of a spool, with actuation components nested inside to vary the bending length, actuate the tendon, and deflect the tip of the guidewire. The spool is mounted onto a lead screw that dispenses the guidewire with a tolerance of ±2 mm. A modified bending joint kinematics and statics model is developed to characterize and validate the relationship between the tendon stroke and the desired curvature. The model is further used in a control system to navigate the distal tip through an *ex vivo* porcine aorta.**

## I. Introduction

Peripheral artery disease (PAD) affects 200 million people worldwide and between 8.5 to 12 million Americans [1]. Atherosclerosis, an inflammatory disease where arteries, typically in the lower extremities, become occluded due to an accumulation of lipids along the arterial wall, accounts for 90% of the cases of PAD [2]. On average, this disease causes about 610,000 deaths every year [3]. A successful treatment for PAD is peripheral vascular intervention (PVI), as it offers a low risk operation, non-invasive physiological tests and imaging techniques [4]. PVIs often involve the placement of a guidewire as a first step. In most cases, guidewires are navigated manually to the target area with the assistance of medical imaging systems. Different guidewires are used during the procedure due to their specific mechanical properties, such as varying stiffness, coatings, and tip flexibility, typically made of steel or nitinol. Superelastic nitinol wires display high strain recovery, thus allowing repeated high curvature bends with minimal damage to the device [5]. Dimensions of commercially available guidewires are range from 0.014" (0.36 mm) to 0.038" (0.97 mm) in diameter and from 80 cm to 450 cm in length [6], [7]. However, traditional guidewires are often hard to manually maneuver through tortuous vessels and arteries, requiring expertise to choose and handle each guidewire [6]. The operator must translate and rotate the wire from outside the patient's body, often with limited use of 2D visual feedback via X-ray fluoroscopy to avoid excess exposure to radiation [8].

Recent advancements in robotic guidewires have been beneficial in minimally invasive surgeries (MIS) [9]. Through the use of computational path planning, along with pre-operative anatomical scans, the guidewires can be robotically steered to the target area without continuous imaging; thus reducing the effects of excessive radiation to both the patient and surgeon. The steerability of robotic guidewires is achieved by the various types of mechanisms, such as precurved concentric tubes [10], [11], magnetically-actuated [12], or tendon-driven robots [13]; in the current work, a tendon-driven guidewire is used. Tendon-driven guidewires usually consist of tubes that are actuated using wires, or "tendons", that when pulled, can bend a flexible region near the distal end of the tube, hence allowing steering capability at the tip.

Tendon-driven guidewires often are limited by the bending joint, where the curvature and angle of bending are coupled. This limitation makes it challenging to traverse vasculature with high angulation without causing trauma to the vessel walls. In our previous work, the COaxially Aligned STeerable (COAST) guidewire was developed with the ability to vary the bending segment length, allowing navigation through phantom vasculature with different curvatures [14]. Using this mechanism, the robotic guidewire can perform follow-the-leader (FTL) motion by keeping a constant curvature along the bending segment of the guidewire. In addition to maneuvering through tortuous vessels in MIS, guidewires need to travel great lengths to reach target areas. The major contributions of this work are as follows:

- A compact advancement mechanism was developed and analyzed consisting of a spool that coils various sizes of nitinol guidewires with the capability of feeding and retracting the guidewire accurately. The design remains compact due to the spooling advancement stage, rather than a linear advancement stage.
- The design specifications of the advancement mechanism were met to feed and retract guidewires up to 150 cm in length (~10 times the length offered by the previous design [14]), and to reduce the overall length of the mechanism.

Research reported in this publication was supported in part by the National Heart, Lung, And Blood Institute of the National Institutes of Health under Award Number R01HL144714. The content is solely the responsibility of the authors and does not necessarily represent the official views of the National Institutes of Health.

The authors are with the Medical Robotics and Automation (RoboMed) Laboratory, Wallace H. Coulter Department of Biomedical Engineering, Georgia Institute of Technology, Atlanta, GA, USA.

*Patrick Lis contributed to the work presented in this paper when he was a graduate student at the Georgia Institute of Technology.

†Grace Trimpe contributed to the work presented in this paper when she was an undergraduate student at the Georgia Institute of Technology. *Corresponding author: Achraj Sarma (achraj@gatech.edu)*

2022 IEEE International Conference on Robotics and Automation (ICRA) | 978-1-7281-9681-7/22/$31.00 ©2022 IEEE | DOI: 10.1109/ICRA46639.2022.9811907

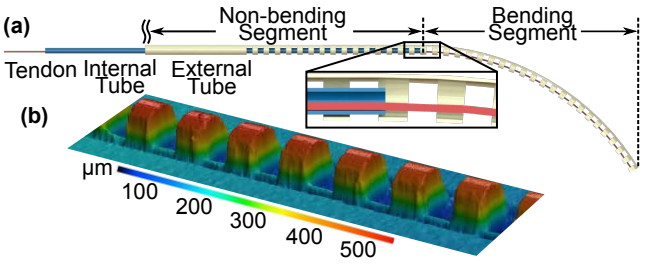


Fig. 1: (a) Modified COAST Guidewire assembly, (inset) Cross-sectional view showing internal structure of the components with an actuated tendon; (b) 3D laser-scanned profile of the external tube.

The paper is organized as follows: First, the mechanical designs are outlined in Section II, starting with a description of the modified COAST guidewire prototype (Section II-A), followed by a detailed discussion of the compact guidewire advancement mechanism (Section II-B), and evaluation of the actuation mechanism components (Section II-C). In Section III, the development of a bending joint kinematics and statics model, along with validation results of the model with experimental data is presented. Maneuvering of the modified COAST robot within *ex vivo* animal vasculature, using the compact guidewire advancement mechanism is presented in Section IV. Finally, conclusions and future work are discussed in Section V.

## II. Mechanical Design

### A. Modified COAST Guidewire Robot

A prototype of the modified COaxially Aligned STeerable (COAST) guidewire robot [14] is constructed using three nitinol components (see Fig. 1(a)). An "external tube", made of superelastic nitinol, is micro-machined using a femtosecond laser (WS-Flex Ultra-Short Pulse Laser Workstation, Optec, Frameries, Belgium) with rectangular unidirectional asymmetric notches to manufacture a compliant joint with a bending segment length of 75 mm. A 3D Surface Profiler (Keyence, IL, United States) was used to accurately measure the notch dimensions (see Fig. 1(b)). Using these calculations, the depth of cut was determined to be 71.04% of the outer diameter, offering a highly compliant bending segment. Within the external tube, an "internal tube", also made of nitinol, is placed to adjust the bending segment length as it is retracted or advanced within the external tube. Within the two tubes, a nitinol wire (Diameter: 0.076 mm) is fixed at the distal tip of the external tube where it can be actuated to achieve a desired curvature. The specifications for all three components for the modified COAST guidewire are shown in Table I. Relative motion between the internal and external tubes allows for the bending segment to be varied depending on the curvature that the guidewire will traverse through. With this structure, the guidewire can be comprised of a 'bending segment' and a 'non-bending segment' (see Fig. 1(a)), where the former is comprised of only the external tube and tendon and latter comprised of all three components. Actuation of the tendon results in a constant curvature profile of the bending segment in the plane of the asymmetric notches as the non-bending segment remains rigid due to the added stiffness of the internal tube. The position of the internal tube dictates how long the bending segment length is while tendon stroke controls the angle of the bending segment joint. The external tube is fixed within the compact guidewire advancement mechanism, while the internal tube independently retracts or advances within the external tube. Within the mechanism there are three controllable variables being:

$$\begin{bmatrix} X_t \\ X_b \\ X_d \end{bmatrix} = \begin{bmatrix} \text{Tendon Stroke} \\ \text{Bending Segment Length} \\ \text{Guidewire Displacement} \end{bmatrix}$$

where $X_t$ controls the length of tendon being pulled to produce desired curvatures, $X_b$ controls the displacement of the internal tube, and $X_d$ controls the displacement of the guidewire in the work space.

TABLE I: Specifications of the modified COAST guidewire prototype.

| Items | External tube | Internal tube | Tendon |
|---|---|---|---|
| Total length (mm) | 417 | 450 | 525 |
| Length of the notched section (mm) | 75.0 | - | - |
| Outer diameter, $2r_o$, (mm) | 0.480 | 0.270 | 0.076 |
| Inner diameter, $2r_i$, (mm) | 0.400 | 0.190 | - |
| $d$ (mm) | 0.341 | - | - |
| $h$ (mm) | 0.290 | - | - |
| $c$ (mm) | 0.270 | - | - |
| Young's modulus (GPa) | 43.000 | 43.000 | 53.965 |

### B. Compact Guidewire Advancement Mechanism

An illustration of the designed mechanism is shown in Fig. 2(a), with the major dimensions shown in Fig. 2(a-1). Though this mechanism is capable of dispensing up to 150 cm of the guidewire, the workspace length of the modified COAST guidewire prototype used for this work was 25 cm. The modified COAST guidewire is placed into a 3D-printed spool (Formlabs, MA, United States) that contains a compact actuation mechanism within to execute desired navigation of the guidewire tip. For the design to remain as compact as possible, the outer diameter of the spool was experimentally determined to be 10 cm. This allows for typical sizes of nitinol guidewires to be coiled around the spool without kinking while allowing all of the internal components to be nested within (see Fig. 2(b)). The guidewire is lead into the spool via a hole 3D-printed within the outer wall of the spool, where a clamp fixes the proximal end of the external tube using bolts, while allowing the internal tube to freely move within it. Following the external tube clamp, the internal tube is passed into the internal tube roller mechanism that controls the bending segment length, $X_b$ (Fig. 2(b)). This action is done using a friction based roller mechanism that utilizes a dual component roller system. The internal tube rests on an aluminum rod driven by a DC motor, with a gear ratio of 380:1 and a nominal torque of 110 mNM, (Pololu Robotics and Electronics, NV, United States) while a 3D-printed free rotating wheel is clamped down onto the aluminum rod using a screw at the exit point of the roller to maintain the right amount of friction between the two rolling segments. The internal tube is retracted 75 mm to

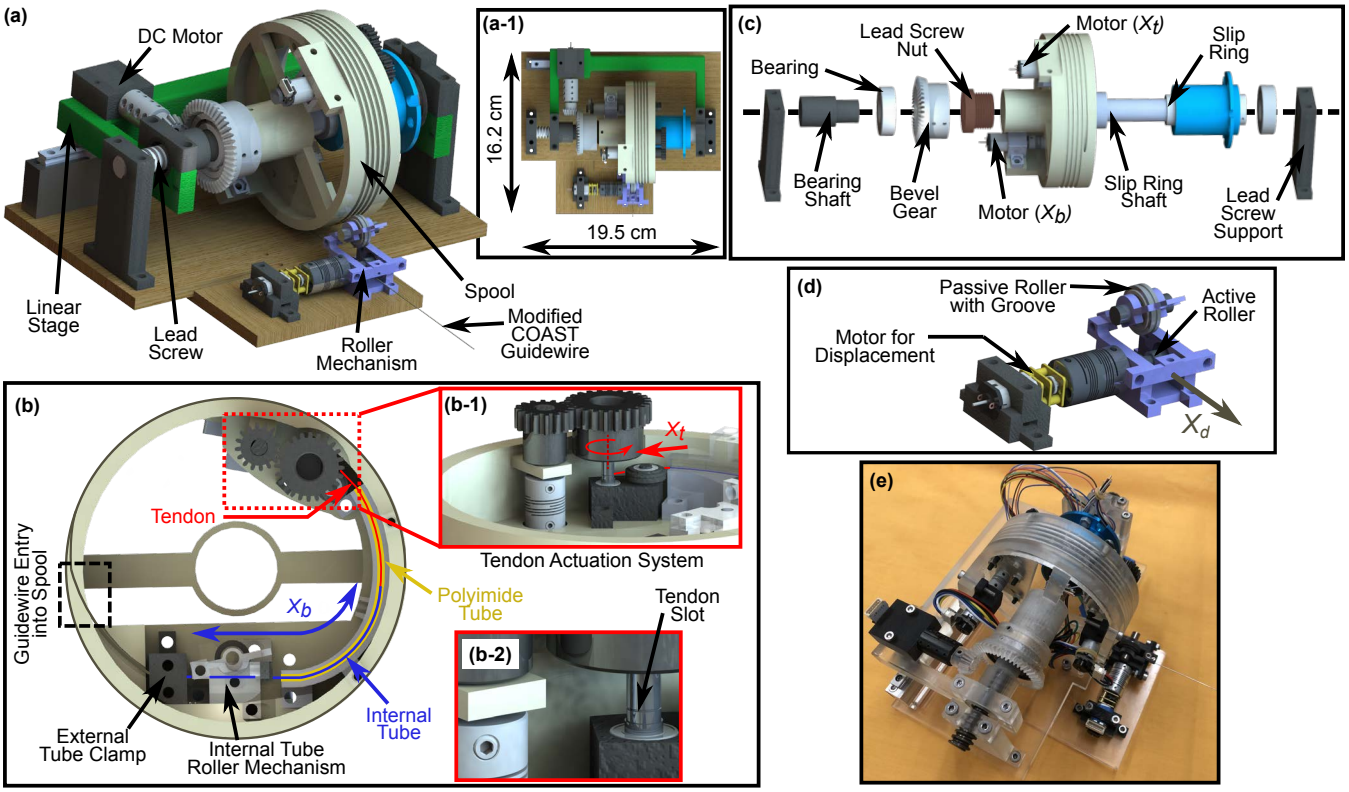


Fig. 2: The compact guidewire advancement mechanism shown with an: (a) Assembled view and a (a-1) Top view of mechanism; (b) Components within the spool mechanism for guidewire tip actuation showing internal tube roller mechanism to control $X_b$, and (b-1) Tendon actuation system to control $X_t$ with (b-2) Close up view of tendon slot for fixed attachment; (c) Exploded view of components mounted onto the lead screw; (d) Assembly of roller mechanism for feeding the guidewire $X_d$; (e) Final build of the compact guidewire advancement mechanism.

allow for the maximum curvature the guidewire can achieve. This internal tube exits the roller and follows a curved path, with an arc length of 75 mm, consisting of a polyimide tube held within a 3D-printed assembly (Fig. 2(b)). The polyimide tube allows the internal tube to slide along the path with little to no interference due to the low coefficient of friction of the material (MicroLumen High Performance Medical Tubing, FL, United States). The internal tube slides along the tendon that is fixed onto an aluminum gear shaft where two spur gears are placed to control the tendon stroke, $X_t$ (Fig. 2(b-1)). The gear shaft is machined with a slot to insert the tendon where it is fixed to actuate the distal tip of the guidewire. This gear mechanism (gear-ratio 3:2) is actuated using a DC motor with a gear ratio of 380:1 and a nominal torque of 110 mNM (Pololu Robotics and Electronics, NV, United States) that pulls the tendon around the gear shaft to produce the desired curvature.

The distal end of the guidewire exits the spool through the internal through-hole to the outside of the spool where a helical path (diameter: 2 mm, pitch: 3 mm/rev) was printed out to hold the guidewire in place, without any overlapping. The spool is then placed onto a lead screw (OD: 12 mm, pitch: 3 mm/rev) via an internal lead nut (length: 195 mm OD: 28.575 mm, ID: 12 mm, pitch: 3 mm/rev) inside the spool hub (Fig. 2(c)). The lead screw is then fixed at the two ends, allowing the spool to rotate via a set of 3D-printed bevel gears (gear-ratio 3:1). The hub of the bevel gear is placed onto the unthreaded part of the lead nut using set screws for the gear to concentrically rotate with the spool along the lead screw. One DC motor (Pololu Robotics and Electronics, NV, United States), with a 380:1 gear ratio and 110 mNm nominal torque, rotates the spool via the bevel gear and pinion system to dispense out the desired length of guidewire. A linear stage is used to translate the DC motor with the spool to ensure the two gears are mated continuously. This linear stage is fixed onto a rail and carriage slide that can move the stage with the spool and maintains proper gear meshing (Fig. 2(a)). The linear stage is connected to both ends of the spool via fixed cylindrical shafts that are held down on each end. To guarantee the spool is rotating freely, two ball bearings (OD: 32 mm, ID: 15 mm) are used so that the spool and components attached to it can revolve around the shafts. One bearing is fixed into the hub of the bevel gear and the other is fixed at the end of the longer shaft. Placed onto the longer shaft is a slip-ring (Senring, Schenzhen, China) that is used to connect the rotating DC motors within the spool to their respective motor drivers. The slip-ring transmits power from a rotating component to a stationary component using a gold contact within. The housing of the slip ring is then fixed to maintain the wires connected to the motor driver stationary outside of the mechanism.

A stationary roller mechanism (Fig. 2(d)) is positioned tangential to where the guidewire exits the spool to hold the guidewire taut and further advance and accurately direct the guidewire into the body. The pitch of the helical path of the

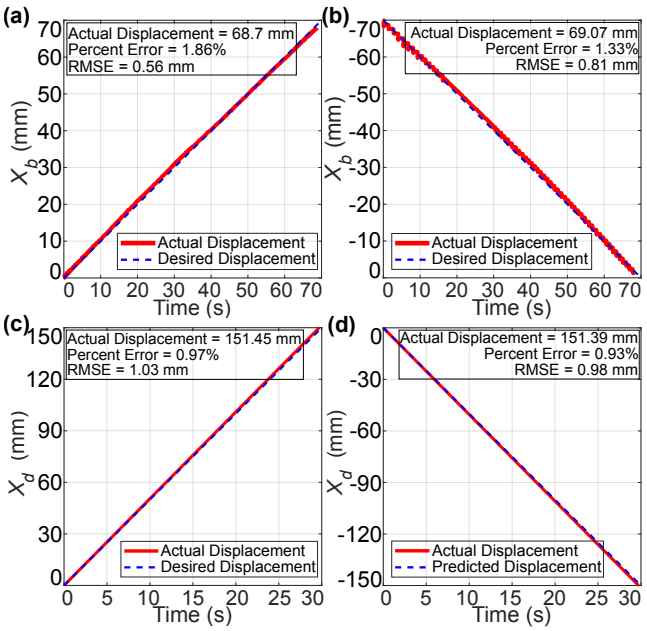


Fig. 3: Evaluation results of inner tube roller mechanism showing (a) advancing, and (b) retracting the inner tube by $X_b = 70$ mm. Evaluation results of guidewire displacement mechanism showing (c) feeding, and (d) retracting the guidewire by $X_d = 150$ mm. Solid red and dashed blue lines indicate actual and desired displacement data, respectively.

spool and the lead screw are identical to ensure the guidewire exiting the advancement mechanism is aligned with the roller mechanism. This friction-based mechanism is fixed onto the same base as the spooling mechanism so the guidewire is always in line with both parts of the mechanism. The active roller is supported by bearings within the two base supports and is driven by a DC Motor with 380:1 gear ratio and a nominal torque of 110 mNm (Pololu Robotics, NV, United States). The top passive roller rotates within the notch of the active roller limiting side to side motion of the guidewire. The top hinged attachment containing the passive roller is fitted into the bottom supports. The passive roller is fixed onto the active roller using a screw, allowing for adjusted pressure on the active roller. Finally, a slot is placed at the distal end of the roller mechanism to further guide the guidewire out into the work space. This component, with its motor on the linear stage are actuated simultaneously to accurately control the guidewire displacement, $X_d$.

### C. Evaluation of Actuation Mechanism Components

To evaluate $X_b$ and $X_d$, an electromagnetic (EM) tracker (Aurora, Northern Digital Inc., Waterloo, Ontario, Canada) was fixed to the distal tip of the guidewire to track its position. Experimental tests were conducted to characterize the two controllable variables. $X_b$ was given an input of 70 mm to advance and retract the internal tube. Fig. 3(a)-(b) display the results for advancing and retracting the internal tube with a percent error less than 2% and an RMSE value of 0.56 mm and 0.81 mm respectively. $X_d$ was given an input of 150 mm and was controlled to feed and retract the guidewire to determine the accuracy of the displacement. Fig. 3(c)-(d) display the results of the guidewire being fed and retracted 150 mm with a percent error less than 1% and an RMSE value of 1.03 mm and 0.98 mm, respectively.

## III. Bending Joint Model

Actuation of the bending segment of the modified COAST robot to a desired curvature, $\kappa$, at a bending length, $X_b$ and for a tendon stroke, $X_t$, was modeled in [14] as:

$$X_t = \underbrace{\Delta L^{kin}(\kappa, X_b)}_{\text{Geometric Stroke}} + \underbrace{\frac{EI_{out}L_{total}}{\Delta y_t E_t \pi r_t^2}\kappa}_{\text{Tendon Elongation}} \quad (1)$$

The detailed expressions for the geometric stroke and tendon elongation terms are derived in our previous work. We note that the prototype of the modified COAST robot does not include a passive outer tube. The middle tube in [14] is considered as the external tube here, and the equations presented are suitably modified. To account for friction within the bending segment due to the tendon-notch interaction, as well as friction losses arising from tendon-pulley interactions within the actuation mechanism, we consider factors for each interaction multiplied with the tendon elongation term as:

$$X_t = \Delta L^{kin}(\kappa, X_b) + \underbrace{e^{\mu\alpha}\eta^{N_f}}_{\text{Friction Loss}} \frac{EI_{out}L_{total}}{\Delta y_t E_t \pi r_t^2}\kappa \quad (2)$$

In the above equation, $\mu$ is the coefficient of friction between the tendon and pulleys in the actuation system, $\alpha$ is the wrapping angle of the tendon around pulleys, $\eta$ is the coefficient of friction between the tendon and notches, $N_f$ is the number of notches in contact with the tendon, $E$ is the Young's modulus of the nitinol tubes, $L_{total}$ is the length of the tendon, $r_t$ is the tendon wire radius, $E_t$ is the Young's modulus of the nitinol tendon wire, $\Delta y_t$ is the moment arm of the tendon at the tip, and $I_{out}$ is the second moment of area of the notched cross-section of the external tube.

To model the bending joint in this paper, we follow a similar outline. The bending joint is assumed to display a constant pre-curvature ($X_t = 0$) and a constant curvature for a tendon stroke input. The geometric stroke term is calculated as $\Delta L^{kin}(\kappa, X_b) = L_i - (L_{cur} + L_{str})$ (as shown in Fig. 4(a), the tendon within the bending segment is divided into curved and tangentially straight section, with arc lengths $L_{cur}$ and $L_{str}$, respectively). However, since the notched length of the middle tube exhibits a machining induced pre-curvature, we estimate the initial length of the tendon, $L_i$, within the bending segment as if it is within an pseudo-actuated bending segment with bending length $X_b$ and the pre-curvature, $\kappa_{pc}$, i.e. $L_i(\kappa_{pc}, X_b) = L_{i,cur} + L_{i,str}$.

The friction interaction due to tendon-notch contact within the bending segment is modeled as $\eta^{N_f}$ ($N_f = (X_b N_{out})/L_{out}^{notch}$ in [15], where the number of notches and the notched section length of the external tube are $N_{out}$ and $L_{out}^{notch}$, respectively). This relation is retained for the current prototype. The friction losses occurring within the actuation mechanism for the tendon contact with curved surfaces are modeled using the Capstan friction model, $e^{\mu\alpha}$. We consider the following interaction regions for estimating the friction within the mechanism:

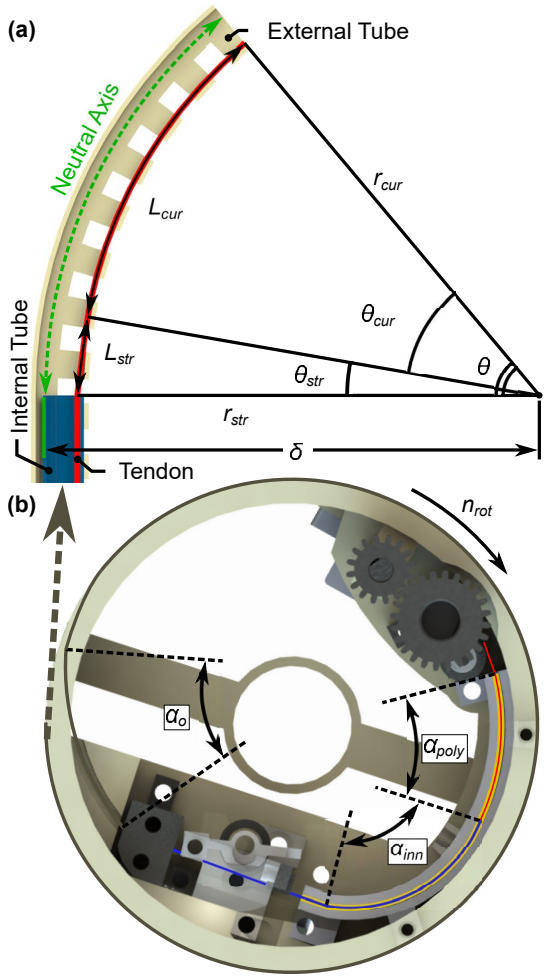


Fig. 4: (a) Sectional view of the bending segment of the modified COAST robot showing geometric parameters (for $\delta = 1/\kappa_{pc}$, initial tendon length $L_i = L_{i,cur} + L_{i,str}$), (b) Spool mechanism components showing wrapping angles for friction loss factors.

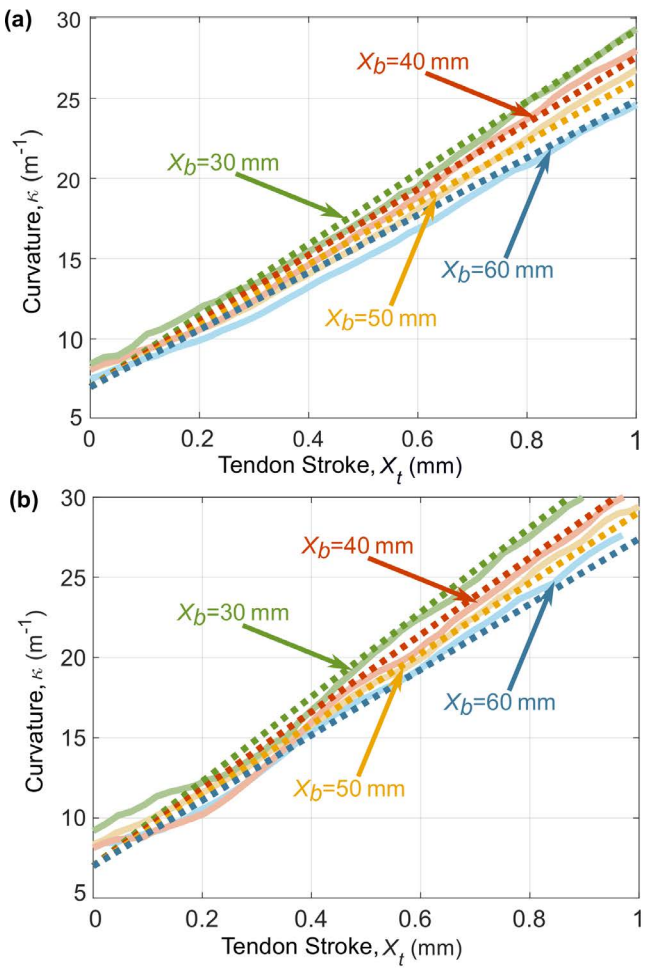


Fig. 5: Joint model validation for various bending segment lengths ($X_b$) at two different guidewire displacements, (a) $X_d$ = 200 mm, and (b) $X_d$ = 250 mm. Solid and dashed lines indicate experimental and modeled data, respectively.

TABLE II: RMSE values ($m^{-1}$), for predicted and experimentally determined curvatures at varying values of $X_d$ and $X_b$

| | $X_b$ (mm) | | | |
|---|---|---|---|---|
| $X_d$ (mm) | 30 | 40 | 50 | 60 |
| 200 | 2.2366 | 0.6016 | 2.0659 | 4.0883 |
| 250 | 2.4512 | 0.8193 | 2.4241 | 4.1360 |

- As the guidewire wraps around the spool, the internal tube is wrapped as well and the wrapping angle is determined as $\alpha_{rot} = n_{rot}.(2\pi)$, where $n_{rot}$ is the number of rotations and is estimated from the total length of the guidewire and the guidewire displacement, $X_d$. The friction loss is then $\exp(\mu_{inn}\alpha_{rot})$, where $\mu_{inn}$ is the coefficient of friction between the tendon and inner surface of the internal tube. As the guidewire is dispensed or spooled up by changing the input $X_d$, $n_{rot}$ decreases or increases, thereby decreasing or increasing the corresponding friction loss term, respectively.
- The curved proximal section of the external tube from the hole in the spool to the clamp (see Section II-B) also includes the internal tube with the tendon sliding within it. Considering the wrapping angle as $\alpha_o$, the friction loss is defined as $\exp(\mu_{inn}\alpha_o)$. The curve of the proximal section of the external tube is maintained throughout the actuation, thereby constraining the internal tube to follow the same curve. Therefore, the wrapping angle, $\alpha_o$, and the corresponding friction loss term are constant.
- As the internal tube is retracted into the curved path to increase the bending length, the tendon again is in contact with the internal tube as well as the polyimide tube. The wrapping angles for both regions, $\alpha_{inn}$ and $\alpha_{poly}$, are evaluated as a function of the bending length $X_b$, and the friction friction loss is $\exp(\mu_{inn}\alpha_{inn} + \mu_{poly}\alpha_{poly})$, where $\mu_{poly}$ is the coefficient of friction between the tendon and polyimide tube. If the inner tube is retracted into the curved path, $\alpha_{inn}$ increases while $\alpha_{poly}$ decreases such that the angle $(\alpha_{inn} + \alpha_{poly})$ is a constant and equal to the total angle of the curved path.

The corresponding wrapping angles are illustrated in Fig. 4(b). The net friction loss factor is computed by taking the product of the above expressions as:

$$\mathscr{F} = \eta^{N_f}.\exp(\mu_{inn}(\alpha_{rot} + \alpha_o + \alpha_{inn})).\exp(\mu_{poly}\alpha_{poly}) \quad (3)$$

Using the modified expression for the geometric stroke, $\Delta L^{kin}_{mod}(\kappa, X_b)$ and replacing the friction loss term in Eq. (2) with (3), we have:

$$X_t = \Delta L^{kin}_{mod}(\kappa, X_b) + \mathscr{F}\frac{E(I_{out})L_{total}}{\Delta y_t E_t \pi r_t^2}\kappa \qquad (4)$$

Validation of the above model was performed by observing the change in curvature ($\kappa$) with varying tendon stroke ($X_t$), while keeping the bending length ($X_b$) and guidewire displacement ($X_s$) constant. The $\kappa - X_t$ trials were performed for varying bending lengths, $X_b = \{30, 40, 50, 60\}$ mm, and this whole set was repeated for two different displacement values. The $\kappa - X_t$ behavior and the joint model data for displacement $X_d = 200$ mm and $X_d = 250$ mm are shown in Fig. 5(a) and 5(b), respectively. The modified COAST guidewire is assembled within the guidewire advancement mechanism such that bending of the distal tip occurs in the horizontal plane. A CMOS Camera (Zelux™ 1.6 MP, Thorlabs Inc., NJ, United States) is mounted above with the lens focusing directly on the bending segment. The curvature for a given tendon stroke input is estimated from the image by fitting a circle subject to the constraint of minimizing the geometric distance [16]. Values of the friction coefficients used to plot the $\kappa$ vs. $X_t$ variation as dictated by the model (Eq. 4) were determined as $\eta = 1.0065$, $\mu_{inn} = 0.2600$, and $\mu_{poly} = 0.7000$. The friction coefficients detailed by the model were manually determined and tuned to reduce the RMSE error between the experimental data and the model. RMSE values for each bending segment length at each guidewire displacement are shown in Table II). We observe an initial non-linear variation for $\kappa$ at lower tendon stroke values. This is attributed to the high compliance of the external tube due to the high depth of cut.

## IV. Demonstration in *ex vivo* Animal Vasculature

The capabilities of the modified COAST guidewire, using the advancement mechanism, are demonstrated by navigation through an *ex vivo* porcine aorta. The experimental setup is shown in Fig. 6(a). Using the model developed in Section III, $X_t$, $X_b$, and $X_d$ were controlled to follow a computed path, imaged from the top plane using an OEC 9800 Plus C-Arm system (GE Healthcare®, Chicago, USA) in which images were acquired using an Orion HD (Matrox™, Dorval, Canada) frame-grabber along with the MATLAB® Image Acquisition Toolbox (MathWorks™, Natick, USA). The path to be traversed was characterized by identifying three parameters $\{a, \delta, \theta\}$: $a$ being the length of the initial straight segment, $\delta$ the radius of curvature of the computed path, and $\theta$ the final bending angle of the curved path. The path was determined by imaging the aorta using the calibrated C-Arm image data. The edges of the curved section of the aorta were found using the Canny edge detection algorithm [17], where the walls of the aorta were identified. The threshold was set to determine the outer wall boundaries and though one of the inner walls was identified (see Fig. 6(a)(inset)), it was ignored. Circular arcs were fit for each of the outer walls of the porcine aorta to determine the corresponding radius of curvature, which was then averaged to determine the radius of curvature of the centerline of the vessel, as shown in Fig. 6(a)(inset). The path parameters for the centerline were determined to be $\{40\,\text{mm}, 159.6\,\text{mm}, 40.45°\}$. The guidewire is observed as it successfully traverses the *ex vivo* animal vasculature as shown in Fig. 6(b-1) through Fig. 6(b-3) along with imaged aorta at the end of the path (Fig. 6(b-3)(close up view)).

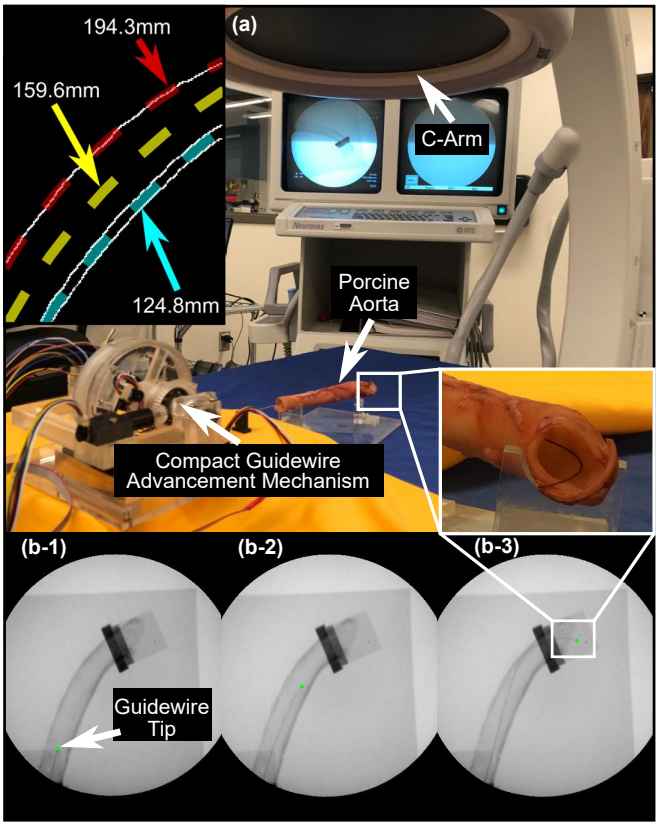


Fig. 6: (a) Experimental setup for *ex vivo* demonstration and (a)(inset) image processing for path parameters. Demonstration of guidewire moving through porcine aorta at the (b-1) beginning, (b-2) middle, and (b-3) end.

## V. Conclusions and Future Work

In this work, a modified COaxially Aligned STeerable (COAST) robotic guidewire was actuated using a novel compact guidewire advancement mechanism that was designed and evaluated to perform one-dimensional FTL motion, using an external tube, an internal tube, and a single tendon for tip deflection. A model of the bending joint kinematics and statics, as well as the friction within the joint and the mechanism, was developed and validated to characterize the system. The model was implemented with an open-loop control approach to demonstrate navigation of the guidewire robot through an *ex vivo* porcine aorta. Future work includes improving the model to account for the non-linear behavior of the bending joint, integration of a passive outer tube to control the pre-curvature of the tip, and using a fluoroscopic imaging (C-Arm) system to obtain visual feedback for improved control. In addition, navigation of successive bends will be demonstrated and analyzed with a longer prototype of the COAST guidewire robot.

## REFERENCES


[1] M. A. Eid, K. S. Mehta, and P. P. Goodney, "Epidemiology of peripheral artery disease," *Seminars in Vascular Surgery*, vol. 34, pp. 38–46, 3 2021.

[2] J. Shu and G. Santulli, "Update on peripheral artery disease: Epidemiology and evidence-based facts," *Atherosclerosis*, vol. 275, pp. 379–381, 8 2018. [Online]. Available: https://pubmed.ncbi.nlm.nih.gov/29843915https://www.ncbi.nlm.nih.gov/pmc/articles/PMC6113064/

[3] R. Pahwa and I. Jialal. (2021, 08) Atherosclerosis. [Online].Available:https://www.ncbi.nlm.nih.gov/books/NBK507799/.[Accessed: September 2, 2021].

[4] A. K. Thukkani and S. Kinlay, "Endovascular intervention for peripheral artery disease," *Circulation Research*, vol. 116, pp. 1599–1613, 4 2015. [Online]. Available: https://pubmed.ncbi.nlm.nih.gov/25908731https://www.ncbi.nlm.nih.gov/pmc/articles/PMC4504240/

[5] A. R. Pelton, T. W. Duerig, and D. Stöckel, "A guide to shape memory and superelasticity in nitinol medical devices," *Minimally Invasive Therapy & Allied Technologies*, vol. 13, pp. 218–221, 1 2004, doi: 10.1080/13645700410017236. [Online]. Available: https://doi.org/10.1080/13645700410017236

[6] C. Walker. (2013, 3) Guidewire selection for peripheral vascular interventions. [Online].Available:https://evtoday.com/articles/2013-may/guidewire-selection-for-peripheral-vascular-interventions.[Accessed: September 2, 2021].

[7] D. Fornell. (2011, 3) The basics of guide wire technology. [Online].Available:https://www.dicardiology.com/article/basics-guide-wire-technology.[Accessed: September 1, 2021].

[8] H. Rafii-Tari, C. J. Payne, and G.-Z. Yang, "Current and emerging robot-assisted endovascular catheterization technologies: A Review," *Annals of Biomedical Engineering*, vol. 42, no. 4, pp. 697–715, 2014.

[9] X. Hu, A. Chen, Y. Luo, C. Zhang, and E. Zhang, "Steerable catheters for minimally invasive surgery: a review and future directions," *Computer Assisted Surgery*, vol. 23, no. 1, pp. 21–41, 2018, pMID: 30497292. [Online]. Available: https://doi.org/10.1080/24699322.2018.1526972

[10] P. Sears and P. Dupont, "A steerable needle technology using curved concentric tubes," in *2006 IEEE/RSJ international conference on intelligent robots and systems*. IEEE, 2006, pp. 2850–2856.

[11] C. Girerd and T. K. Morimoto, "Design and control of a hand-held concentric tube robot for minimally invasive surgery," *IEEE Transactions on Robotics*, vol. 37, no. 4, pp. 1022–1038, 2021.

[12] J. Kim, P. B. Nguyen, B. Kang, E. Choi, J.-O. Park, and C.-S. Kim, "A novel tip-positioning control of a magnetically steerable guidewire in sharply curved blood vessel for percutaneous coronary intervention," *International Journal of Control, Automation and Systems*, vol. 17, no. 8, pp. 2069–2082, 2019.

[13] Y. Chitalia, X. Wang, and J. P. Desai, "Design, modeling and control of a 2-dof robotic guidewire," in *2018 IEEE International Conference on Robotics and Automation (ICRA)*. IEEE, 2018, pp. 32–37.

[14] S. Jeong, Y. Chitalia, and J. P. Desai, "Design, modeling, and control of a coaxially aligned steerable (COAST) guidewire robot," *IEEE Robotics and Automation Letters*, vol. 5, pp. 4947–4954, 2020.

[15] A. Sarma, T. Brumfiel, Y. Chitalia, and J. P. Desai, "Kinematic modeling and Jacobian-based control of the COAST guidewire robot," *IEEE Robotics and Automation Letters*, (*Submitted*).

[16] W. Gander, G. H. Golub, and R. Strebel, "Least-squares fitting of circles and ellipses," *BIT Numerical Mathematics*, vol. 34, no. 4, pp. 558–578, 1994.

[17] J. Canny, "A computational approach to edge detection," *IEEE Transactions on Pattern Analysis and Machine Intelligence*, vol. PAMI-8, no. 6, pp. 679–698, 1986.